

What do physics-informed DeepONets learn? Understanding and improving training for scientific computing applications

Emily Williams^{1,2}, Amanda Howard¹, Brek Meuris³, and Panos Stinis¹

¹Advanced Computing, Mathematics and Data Division, Pacific Northwest
National Laboratory, WA 99354

²Massachusetts Institute of Technology, MA 02139

³Sandia National Laboratories, NM 87123

November 28, 2024

Abstract

Physics-informed deep operator networks (DeepONets) have emerged as a promising approach toward numerically approximating the solution of partial differential equations (PDEs). In this work, we aim to develop further understanding of what is being learned by physics-informed DeepONets by assessing the universality of the extracted basis functions and demonstrating their potential toward model reduction with spectral methods. Results provide clarity about measuring the performance of a physics-informed DeepONet through the decays of singular values and expansion coefficients. In addition, we propose a transfer learning approach for improving training for physics-informed DeepONets between parameters of the same PDE as well as across different, but related, PDEs where these models struggle to train well. This approach results in significant error reduction and learned basis functions that are more effective in representing the solution of a PDE.

1 Introduction

In recent years, physics-informed deep learning has emerged as a viable approach for the numerical solution of partial differential equations (PDEs) [23, 18, 1]. The deep operator network (DeepONet) consists of a deep neural network (DNN) for encoding the discrete input function space (branch net) and another DNN for encoding the domain of the output functions (trunk net) [22]. Physics-informed DeepONets leverage automatic differentiation to impose the underlying physical laws during model training [30]. The use of the neural tangent kernel (NTK) to assign weights dynamically for the terms in the loss function used to train the DeepONet has demonstrated improved predictions compared with using fixed predetermined weights [24, 29]. However, further investigation is warranted toward understanding and improving training for physics-informed DeepONets [29].

Further, we want to investigate the benefits in exploiting physics-informed DeepONets toward improving traditional scientific computing methods. DeepONets can be used to identify custom-made candidate basis functions on which to expand the solution of PDEs for evolution using a spectral approach [23]. In this work, we assess the applicability of the basis functions extracted from data-driven and physics-informed DeepONets. Then, we propose a transfer learning approach to initializing physics-informed models for PDEs where these models fail to train well.

2 Technical Approach

2.1 Data-driven and physics-informed DeepONets

Consider a time-dependent PDE

$$s_t + \mathcal{N}[s] = 0 \quad (1)$$

with appropriate boundary conditions and initial condition $s(x, 0) = u(x)$. The goal is to learn the continuous, possibly nonlinear, solution operator $\mathcal{G} : u(x) \mapsto s(x, t)$. The universal approximation theorem guarantees the existence of a pair of 2-layer neural networks such that the inner product of their outputs can approximate the action of a continuous nonlinear operator to arbitrary accuracy [22, 4].

$$\mathcal{G}(u)(y) \approx \sum_{k=1}^w b_k(\underbrace{u(x_1), u(x_2), \dots, u(x_m)}_{\text{branch}}) \underbrace{\gamma_k(y)}_{\text{trunk}} \quad (2)$$

A DeepONet $\mathcal{G}_{NN}(u)(y)$ is a deep neural architecture designed to approximate \mathcal{G} evaluated at $y = (x, t)$. It takes as inputs a discrete representation $u = (u(x_j))_{1 \leq j \leq m}$, where x_1, \dots, x_m are pre-selected sensor points, and an output location $y = (x, t)$ in the spatiotemporal domain. The DeepONet consists of deep branch and trunk networks $\{b_k\}_{1 \leq k \leq w}$ and $\{\gamma_k\}_{1 \leq k \leq w}$ merged together in a dot product layer

$$\mathcal{G}_{NN}^\theta(u)(y) = \sum_{k=1}^w b_k(u) \gamma_k(y) \quad (3)$$

where θ denotes the trainable parameters. Given N input-output function pairs $\{(u^{(j)}, s^{(j)})\}_{1 \leq j \leq N}$, where $s^{(j)} = \mathcal{G}(u^{(j)})$, and P corresponding evaluation points $\{y_i^{(j)}\}_{1 \leq i \leq P, 1 \leq j \leq N}$, this architecture is trained by minimizing the mean-squared error as the loss function

$$\mathcal{L}(\theta) = \frac{1}{NP} \sum_{j=1}^N \sum_{i=1}^P \left(s^{(j)}(y_i^{(j)}) - \mathcal{G}_{NN}^\theta(u^{(j)})(y_i^{(j)}) \right)^2 \quad (4)$$

For each input function u , the same number and location of the sensor points is required. There are no constraints on the number or locations for the evaluation of the output functions.

Physics-informed DeepONets recognize that the outputs of a DeepONet model are differentiable with respect to their input coordinates. This enables the use of automatic differentiation to formulate an appropriate regularization mechanism for biasing the target output functions to satisfy the underlying physical constraints. Then, we have a procedure for training physics-informed DeepONet models without requiring any training data for the latent output functions, except for the appropriate initial and boundary conditions of a given PDE system [30].

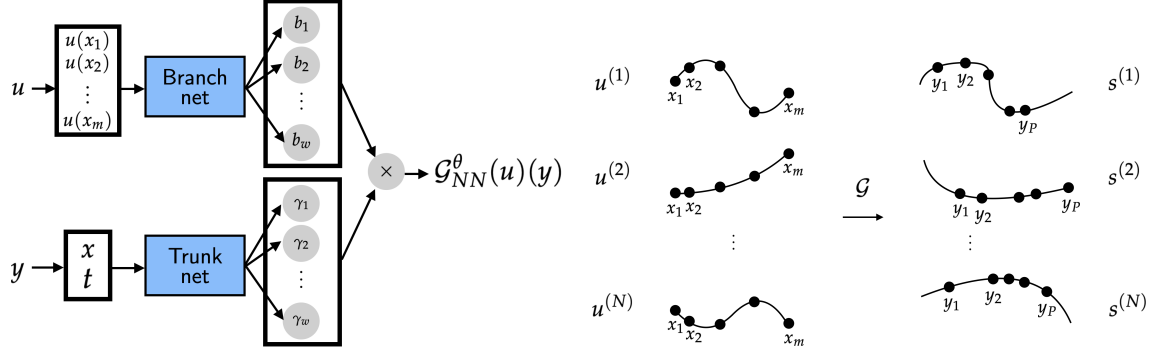


Figure 1: DeepONet architecture and training (adapted from [22]).

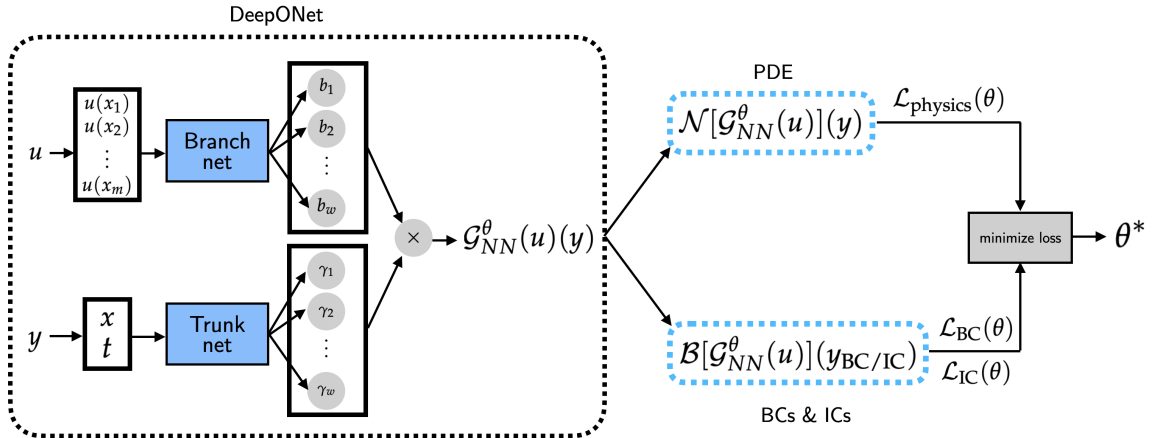


Figure 2: Physics-informed DeepONet (adapted from [30]).

2.2 Transfer learning for initialization

Transfer learning refers to exploiting what has been learned in one problem to improve generalization in a different, but related, problem [10, 3, 6]. Transfer learning has been shown to decrease the training time for a DNN while also resulting in lower generalization error for tasks in computer vision and natural language processing, for example, that require lengthy training times with large amounts of training data [25, 5, 21, 15, 26]. Initialization of DNNs can have a substantial impact on convergence during training [9]. Initializing a new model with weights from a previously trained model is called fine-tuning and has been shown to result in improved performance compared to random initialization [34, 35, 32]. Transfer learning has been increasingly used in operator learning models. Recent work has included fine-tuning DeepONets to result in lower training times for transferring and evolving knowledge [33, 11, 27]. The capability of DeepONets have been extended to train for multiple tasks on multiple domains and geometries with the aid of transfer learning [19, 17, 14]. However, the choice of initialization in particular and the tasks that benefit from transfer initialization by weights is still not well understood, especially for physics-informed

problems [10, 31, 11]. We use transfer learning for the initialization of the weights and biases for physics-informed DeepONets from previously trained models. This is demonstrated for the same PDE across different parameters, as well as across different, but related, PDEs.

2.3 Neural tangent kernel

The neural tangent kernel (NTK) is a framework for better convergence and generalization guarantees for DNNs [16, 7, 2]. For physics-informed DeepONets, the NTK is used to assign weights dynamically for each term in the loss function (e.g., ICs/BCs, PDE) for each evaluation point and for each training iteration [29, 24]. As above and following [29], a physics-informed DeepONet is trained by minimizing

$$\mathcal{L}(\theta) = \mathcal{L}_{\text{BC/IC}}(\theta) + \mathcal{L}_{\text{PDE}}(\theta) = \frac{2}{N^*} \sum_{k=1}^{N^*} \left(\mathcal{T}^{(k)} \left(u^{(k)}(x_k), \mathcal{G}_{\text{NN}}^\theta \left(u^{(k)} \right) (y_k) \right) \right)^2 \quad (5)$$

where $N^* = 2NP$. For every k , $\mathcal{T}^{(k)}(\cdot, \cdot)$ can be the identity operator, differential operator \mathcal{N} , or boundary condition \mathcal{B} . This form of the loss function is "fully-decoupled" [29]. Given this loss function, the NTK is a matrix $\mathbf{H}(\theta) \in \mathbb{R}^{N^* \times N^*}$ with entries

$$\mathbf{H}_{ij}(\theta) = \left\langle \frac{\mathcal{T}^{(i)} \left(u^{(i)}(x_i), \mathcal{G}_{\text{NN}}^\theta \left(u^{(i)} \right) (y_i) \right)}{d\theta}, \frac{\mathcal{T}^{(j)} \left(u^{(j)}(x_j), \mathcal{G}_{\text{NN}}^\theta \left(u^{(j)} \right) (y_j) \right)}{d\theta} \right\rangle \quad (6)$$

for $i, j = 1, 2, \dots, N^*$. For NTK-guided weights, consider the weighted loss function

$$\mathcal{L}(\theta) = \frac{2}{N^*} \sum_{k=1}^{N^*} \lambda_k \left(\mathcal{T}^{(k)} \left(u^{(k)}(x_k), \mathcal{G}_{\text{NN}}^\theta \left(u^{(k)} \right) (y_k) \right) \right)^2 \quad (7)$$

All weights $\{\lambda_k\}_{k=1}^{N^*}$ are initialized to 1 and updated during training by

$$\lambda_k = \left(\frac{\|\mathbf{H}(\theta)\|_\infty}{\mathbf{H}_{kk}(\theta_n)} \right)^\alpha \quad (8)$$

where θ_n denotes the DeepONet parameters at step n . Here, α is a hyper-parameter that determines the magnitude of each weight. From [29], $\alpha = 1$ refers to local NTK weights while $\alpha = 1/2$ refers to moderate local NTK weights. Using NTK-guided weights for the loss function was shown to result in higher prediction accuracy for the physics-informed DeepONet when compared to fixed predetermined weights.

A disadvantage of the NTK is that it can greatly increase the computational time for training a physics-informed DeepONet, and in some cases the NTK is intractable due to having to propagate through a large network. The conjugate kernel (CK) is the kernel induced by the Jacobian only with respect to the parameters θ in the last layer [24, 8]. The CK can be thought of as a zeroth-order approximation to the NTK [24]. Using CK-guided weights has been shown to result in increased efficiency and accuracy for training physics-informed DeepONets for many applications, although the NTK can have better convergence for some PDEs [12].

2.4 Basis functions for spectral methods

The custom basis functions are extracted from the trunk net function space using a singular value decomposition (SVD) based method. Following [23], we denote the collection of “frozen-in-time” trunk net functions by $\{\tau_k\}_{1 \leq k \leq p}$, e.g., by evaluating the trunk net functions $\{\gamma_k\}$ at $t = 0$ (so that $p = w$, where w is the width of the trunk net output used in the DeepONet representation).

Denote by $\langle \cdot, \cdot \rangle$ the L^2 inner product on a spatial domain Ω and let $\{(x_i, \omega_i)\}_{1 \leq i \leq M}$ be a quadrature rule on Ω so that $\langle h_1, h_2 \rangle \approx \sum_{i=1}^M \overline{h_1(x_i)} h_2(x_i) \omega_i$. The eigenfunctions $\{\phi_k\}_{1 \leq k \leq p}$ of the covariance operator

$$\mathcal{C} = \sum_{k=1}^p \tau_k \otimes \tau_k = \sum_{k=1}^p \tau_k \langle \tau_k, \cdot \rangle, \quad (9)$$

ordered by decreasing eigenvalues, form an orthonormal basis for $\mathcal{S} = \text{span}(\{\tau_k\}_{1 \leq k \leq p})$. Discretizing \mathcal{C} and performing its eigendecomposition to compute the basis functions is computationally infeasible. Instead, define the $M \times p$ matrix B by $B_{ik} = \omega_i^{1/2} \tau_k(x_i)$ and perform its SVD $B = QSV^*$. Letting $W = \text{diag}(\omega_1, \dots, \omega_M)$, the entries of $W^{-1/2}Q$ provide the values of $\{\phi_k\}$ at the quadrature points via

$$\phi_k(x_i) = (W^{-1/2}Q)_{ik} \text{ for } 1 \leq i \leq M \text{ and } 1 \leq k \leq p \quad (10)$$

The functional forms of the basis functions need to be recovered to allow for their usage in a spectral method, such as through an orthogonal polynomial expansion. For any $\tilde{M} < M$, let $\{L_j\}_{0 \leq j \leq \tilde{M}}$ be the orthonormal Legendre polynomials on Ω and define the functions $\{\tilde{\phi}_k\}_{1 \leq k \leq p}$ by

$$\tilde{\phi}_k = \sum_{j=0}^{\tilde{M}} \left(\sum_{i=1}^M L_j(x_i) \phi_k(x_i) \omega_i \right) L_j \quad (11)$$

This procedure proposed by [23] only uses well-conditioned operations to obtain a projection enabling the evaluation of the basis functions. By choosing a sufficiently large \tilde{M} , the $\{\tilde{\phi}_k\}$ serve as good approximations to $\{\phi_k\}$. The singular values $S = \text{diag}(\sigma_1, \dots, \sigma_p)$ signify the contribution of each basis function to \mathcal{S} . Only using basis functions corresponding to singular values greater than a specified cutoff, typically 10^{-13} , leads to more robust solutions, since the noisy functions are weeded out, for cheaper computational cost in a spectral approach [23]. Consider the weak formulation for a time-dependent PDE

$$\langle \tilde{\phi}_k, s_t + \mathcal{N}[s] \rangle = 0 \quad (12)$$

for $1 \leq k \leq p$. Express the solution as a linear combination

$$\hat{s} = \sum_{i=1}^p a_i(t) \tilde{\phi}_i(x) \quad (13)$$

Substituting this approximation into the weak formulation results in a system of ordinary differ-

ential equations (ODEs) for the expansion coefficients

$$a'_k(t) = - \left\langle \tilde{\phi}_k, \mathcal{N} \left[\sum_{i=1}^p a_i(t) \tilde{\phi}_i \right] \right\rangle \quad (14)$$

$$a_k(0) = \langle \tilde{\phi}_k, u \rangle = \sum_{j=1}^M \tilde{\phi}_k(x_j) u(x_j) \omega_j \quad (15)$$

3 Results

3.1 Advection-diffusion

We first demonstrate the use of physics-informed basis functions in a spectral method, comparing to the effectiveness of the data-driven custom basis functions [23]. Consider the advection-diffusion equation

$$\frac{\partial s}{\partial t} + \alpha \frac{\partial s}{\partial x} - \nu \frac{\partial^2 s}{\partial x^2} = 0 \quad (16)$$

on $(x, t) \in (0, 2\pi) \times (0, 1)$ with periodic boundary conditions. The advection coefficient is $\alpha = 4$ and the diffusion coefficient is $\nu = 0.01$. The goal is to learn the solution operator $\mathcal{G} : u(x) \mapsto s(x, t)$, where the input to the branch network is the initial condition $s(x, 0) = u(x) \sim$ Gaussian random field (GRF).

To show the difference between data-driven and physics-informed training, we train both with data from a solution field computed using a Fourier pseudo-spectral method and with a physics-informed loss function, which does not use data. The data-driven and physics-informed DeepONets with fixed weights use the MLP architecture as in [23]. The physics-informed DeepONet trained with local NTK adaptive weights uses the modified DeepONet architecture with an additional hidden layer [29]. Figure 3 shows the reference solution field generated by the Fourier method for one independent test sample initial condition and the predictions from the data-driven and physics-informed (NTK) DeepONets. Qualitatively, the approximations show agreement with the solution. Table 1 quantifies the average relative ℓ_2 errors for the data-driven, physics-informed with fixed weights, and physics-informed with local NTK adaptive weights compared with the reference solution. The relative ℓ_2 error is calculated as in Equation 17, where \hat{s} is the approximation and s is the reference. This error is integrated over time to calculate the average relative ℓ_2 error (see Appendix E). All models approximate the solution well, within 1% error. Importantly, for this problem, the physics-informed training is almost as accurate as data-driven training.

$$E(t_n) = \frac{\|\hat{s}(x, t_n) - s(x, t_n)\|_2}{\|s(x, t_n)\|_2} \quad (17)$$

The singular values accompanying each basis function provide a measure of the contribution of each function to the trunk net function space [23]. The decay of the expansion coefficients, calculated by $a_k = \langle \tilde{\phi}, f \rangle$ for function $f = e^{\sin(x)}$, relates to the accuracy of the trained model. Figure 4 shows the decay of the singular values and the expansion coefficients for the DeepONets trained for advection-diffusion. The expansion coefficients of all the trained models decay to machine

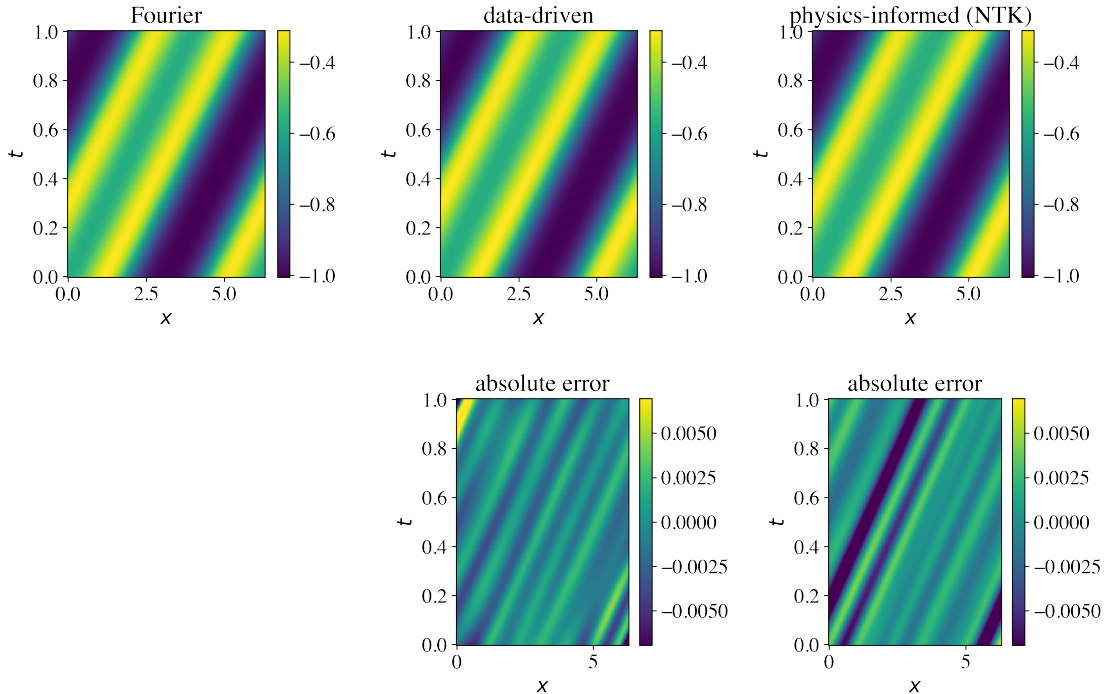


Figure 3: (Left) Fourier reference solution field, (middle) data-driven, (right) physics-informed DeepONet predictions for advection-diffusion. The absolute error is calculated as $\hat{s} - s$.

	w	Average relative ℓ_2 error
data-driven	128	0.44% \pm 0.32%
physics-informed (fixed)	128	0.48% \pm 0.41%
physics-informed (NTK)	128	0.82% \pm 0.54%

Table 1: Average errors across 100 test samples for advection-diffusion.

precision. The singular values of the basis functions extracted from the physics-informed model trained with NTK adaptive weighting show faster decay than those from the physics-informed DeepONet model with fixed weights and the data-driven DeepONet model. When DeepONets train well, evident through the decay of the expansion coefficients, then the decay of the singular values shows the degrees of freedom that are important in representing the solution space. A sample of the custom basis functions is shown in Figure 5. The basis functions (except for $k = 0$) show good agreement across all the models (data-driven and physics-informed), demonstrating potential universality in what is learned by DeepONets during the training process. The first 10 custom basis functions can be found in Appendix C.1.

Then, following [23], we can use the basis functions from the physics-informed DeepONet with NTK-guided weights in evolving the approximation using a spectral approach. Corresponding to

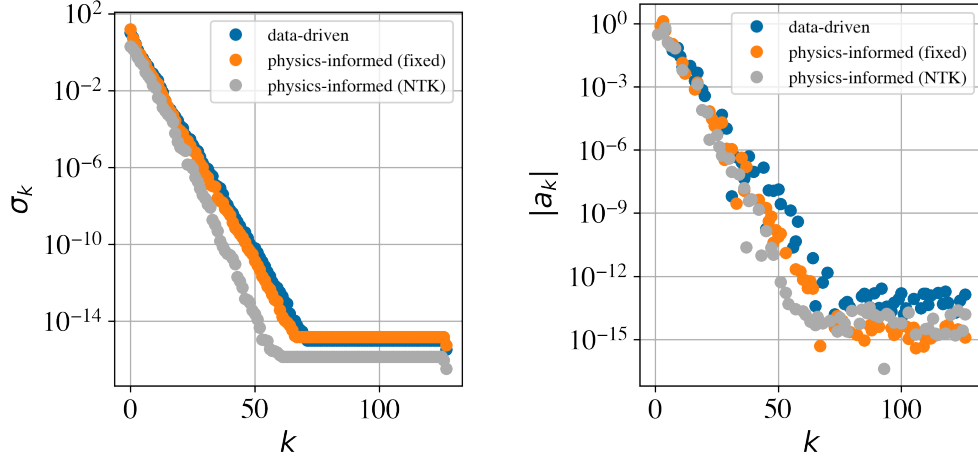


Figure 4: (Left) Singular values and (right) expansion coefficients $e^{\sin(x)}$ for data-driven and physics-informed DeepONets for advection-diffusion.

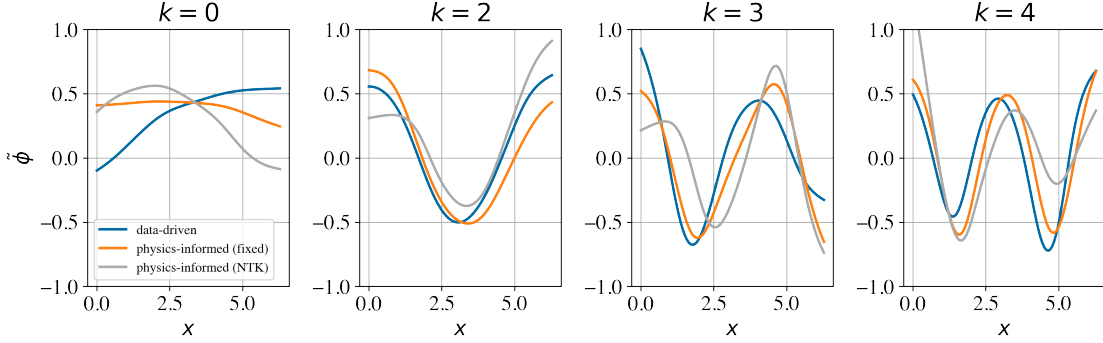


Figure 5: Custom basis functions, plotting with consistent boundaries $\tilde{\phi}(x = 0 \text{ or } 2\pi)$ for advection-diffusion.

singular values greater than the specified cutoff of 10^{-13} , we use 62 data-driven custom basis functions to approximate the solution. For this same cutoff, we only require 47 physics-informed custom basis functions. The approximation fields from the test initial condition are shown in Figure 6. The top plots of Figure 7 show the relative ℓ_2 errors as we use more custom basis functions in generating the solution field, approaching each respective cutoff, for data-driven and physics-informed. The errors in time are relatively consistent and decrease overall as we use more basis functions. As the cutoff is approached, the errors saturate. From the bottom plot, using the custom basis functions from the physics-informed DeepONet results in lower error. Shown in Table 2, we reach the same magnitude of the average relative ℓ_2 error of 10^{-7} for both data-driven and physics-

informed custom spectral approximations. However, we only require 47 physics-informed custom basis functions to reach this error compared to 62 data-driven custom basis functions. From this, we can see that data-driven and physics-informed DeepONets train to a similar relative error for this equation. However, when considering using the learned DeepONet basis functions in a spectral method, the physics-informed DeepONet representation used 25% fewer basis functions to reach the same relative error. This suggests that the physics-informed basis functions are more effective in representing the solution space for this linear PDE.

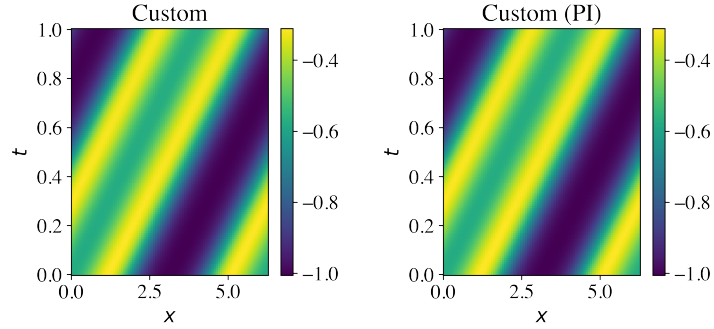


Figure 6: Spectral evolution with (left) 62 data-driven and (right) 47 physics-informed custom basis functions for advection-diffusion.

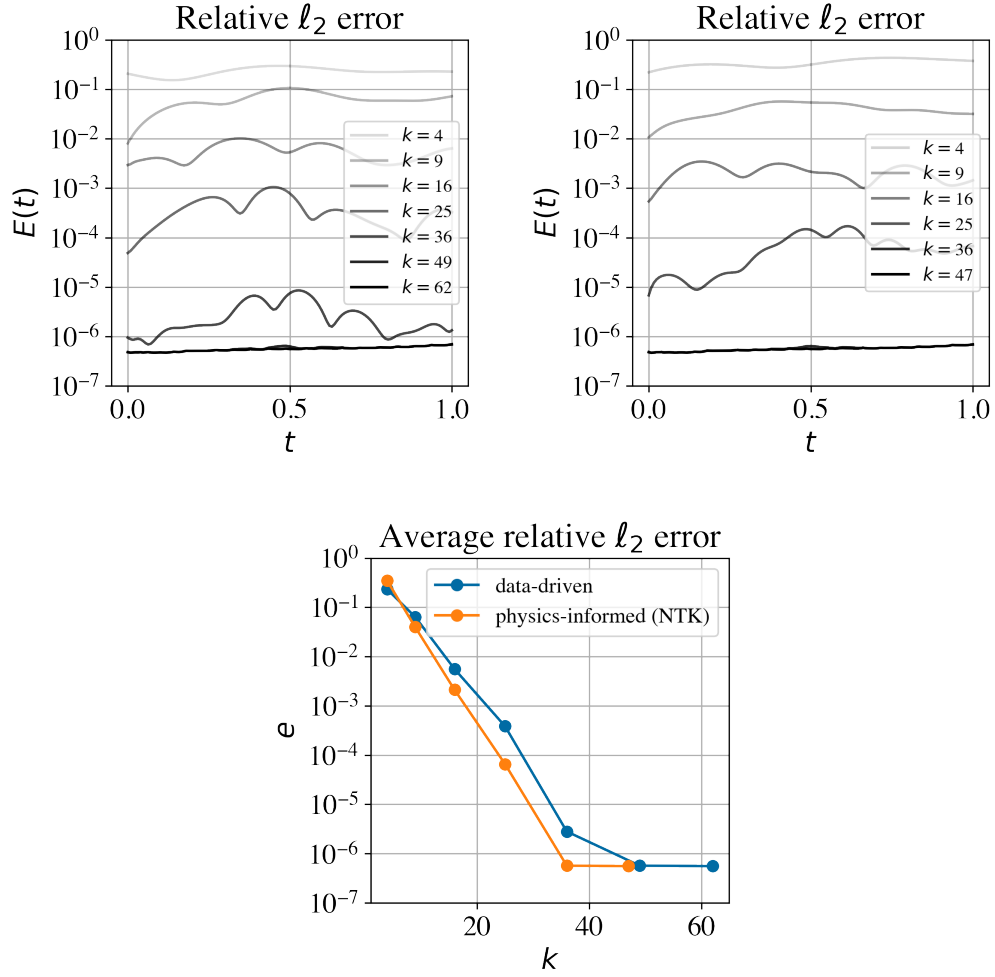


Figure 7: (Top left) Relative data-driven, (top right) relative physics-informed, and (bottom) average relative ℓ_2 test sample errors for random test sample initial condition with k custom basis functions for advection-diffusion.

	p	Average relative ℓ_2 error
data-driven	62	5.767×10^{-7}
physics-informed (NTK)	47	5.576×10^{-7}

Table 2: Average errors for independent test sample for advection-diffusion.

3.2 Viscous Burgers

The viscous Burgers equation has become a standard benchmark for physics-informed DeepONets [30, 29]. While physics-informed DeepONets train well for high viscosities ($\nu = 0.1, 0.01$), they can struggle to train for low viscosities ($\nu = 0.0001$), making this benchmark an interesting case to understand physics-informed DeepONet training. See Appendix D for a cost assessment for training with different weighting schemes for the viscous Burgers benchmark case.

3.2.1 $\nu = 0.1$

Consider the viscous Burgers equation

$$\frac{\partial s}{\partial t} + s \frac{\partial s}{\partial x} - \nu \frac{\partial^2 s}{\partial x^2} = 0 \quad (18)$$

on $(x, t) \in (0, 2\pi) \times (0, 1)$ with periodic boundary conditions. The viscosity coefficient is $\nu = 0.1$. The input to the branch network is the initial condition $s(x, 0) = u(x)$. For data-driven training and for calculating errors, the solution field is computed using a Fourier pseudo-spectral method. The goal is to learn the solution operator $\mathcal{G} : u(x) \mapsto s(x, t)$. The data-driven and physics-informed DeepONets with fixed weights use the MLP architecture as in [23]. The physics-informed DeepONet trained with moderate local NTK adaptive weights uses the modified DeepONet architecture [29]. Figure 8 shows the reference solution field generated by the Fourier method for one independent test sample initial condition and the predictions from the data-driven and physics-informed (NTK) DeepONets. Table 3 quantifies the average relative ℓ_2 errors for the data-driven, physics-informed with fixed weights, and physics-informed with moderate local NTK adaptive weights compared with the reference solution. The physics-informed model with the NTK outperforms the physics-informed with fixed weights and the data-driven models.

	w	Average relative ℓ_2 error
data-driven	128	$1.98\% \pm 1.22\%$
physics-informed (fixed)	128	$4.48\% \pm 3.00\%$
physics-informed (NTK)	128	$1.20\% \pm 1.06\%$

Table 3: Average errors across 100 test samples for viscous Burgers with $\nu = 0.1$.

Figure 9 shows the decay of the singular values and the expansion coefficients for the DeepONets trained for viscous Burgers with $\nu = 0.1$. The singular values of the basis functions extracted from the physics-informed model trained with NTK adaptive weighting show significantly faster decay than those from the physics-informed DeepONet model with fixed weights and the data-driven DeepONet model. The expansion coefficients of all the trained models decay to machine precision, showing that the models are training effectively. Therefore, the decay of the singular values shows the degrees of freedom that are important in capturing the solution space. A sample of the custom basis functions is shown in Figure 10. Again, except for $k = 0$, the agreement of the basis functions demonstrate the universality in what might be learned by DeepONets. The first 10 custom basis functions can be found in Appendix C.2.1.

We can use these basis functions in evolving the approximation using a spectral approach, with 106 data-driven custom basis functions and 67 physics-informed custom basis functions. The approximation fields are shown in Figure 11. Figure 12 shows the relative ℓ_2 errors and average

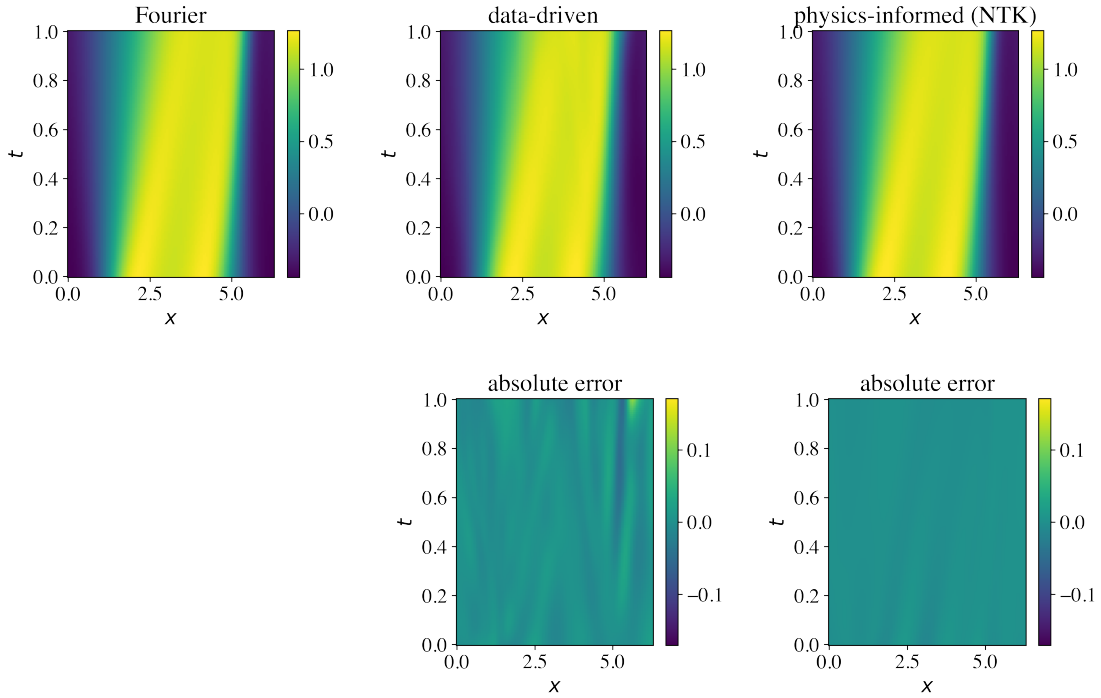


Figure 8: (Left) Fourier reference solution field, (middle) data-driven, and (right) physics-informed (NTK) DeepONet predictions for viscous Burgers with $\nu = 0.1$. The absolute error is calculated as $\hat{s} - s$.

relative ℓ_2 error for the data-driven and physics-informed custom basis functions as we approach the cutoff in the singular value decay, where the errors eventually saturate. The decay of the error for the physics-informed model with NTK-guided weights is shown to be comparable to the Fourier method. Shown in Table 4, we achieve the same magnitude of the average relative ℓ_2 error of 10^{-6} with 106 data-driven custom basis functions and only 67 physics-informed custom basis functions.

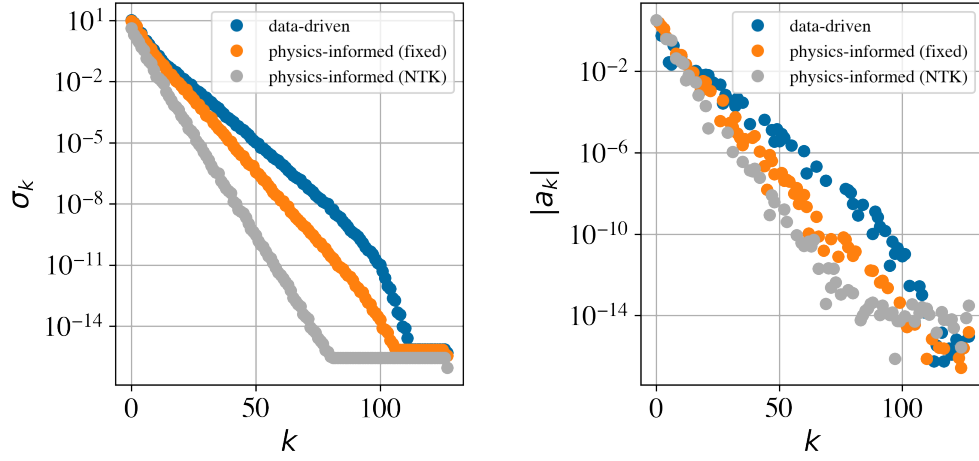


Figure 9: (Left) Singular values and (right) expansion coefficients $e^{\sin(x)}$ for data-driven and physics-informed DeepONets for viscous Burgers with $\nu = 0.1$.

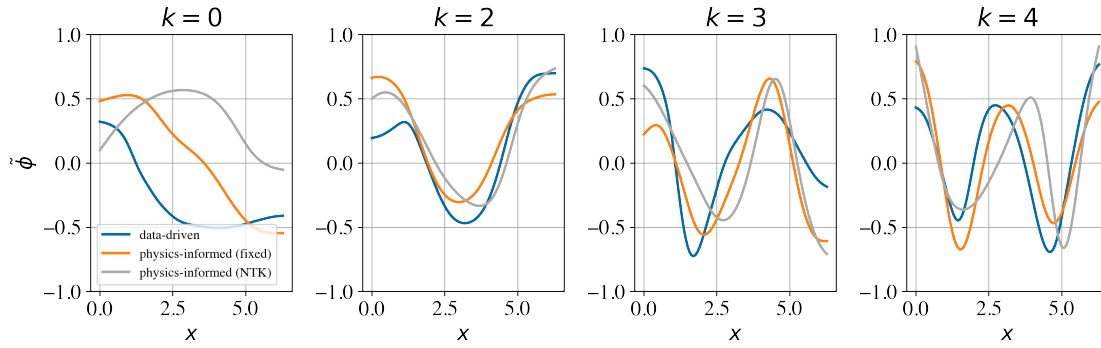


Figure 10: Custom basis functions, plotting with consistent boundaries $\tilde{\phi}(x = 0 \text{ or } 2\pi)$ for viscous Burgers with $\nu = 0.1$.

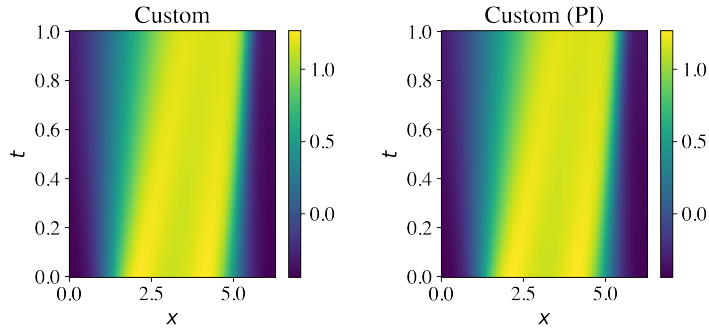


Figure 11: Spectral evolution with (left) data-driven and (right) physics-informed custom basis functions for viscous Burgers with $\nu = 0.1$.

These results show that improving physics-informed DeepONets training, such as by using adaptive weighting like that based on NTK, could have model reduction benefits for smooth problems. Moreover, for nonlinear problems, enforcing the physics during training does have a substantial impact. These benefits are evident through assessing the decay of the singular value spectrum as well as the drop in the values of the expansion coefficients. For models that train well and require fewer degrees of freedom to capture the solution space, we can exploit the advantages in constructing a more robust collection of basis functions for use in a spectral method.

	p	Average relative ℓ_2 error
data-driven	106	1.537×10^{-6}
physics-informed (NTK)	67	1.548×10^{-6}

Table 4: Average errors for independent test sample for viscous Burgers with $\nu = 0.1$.

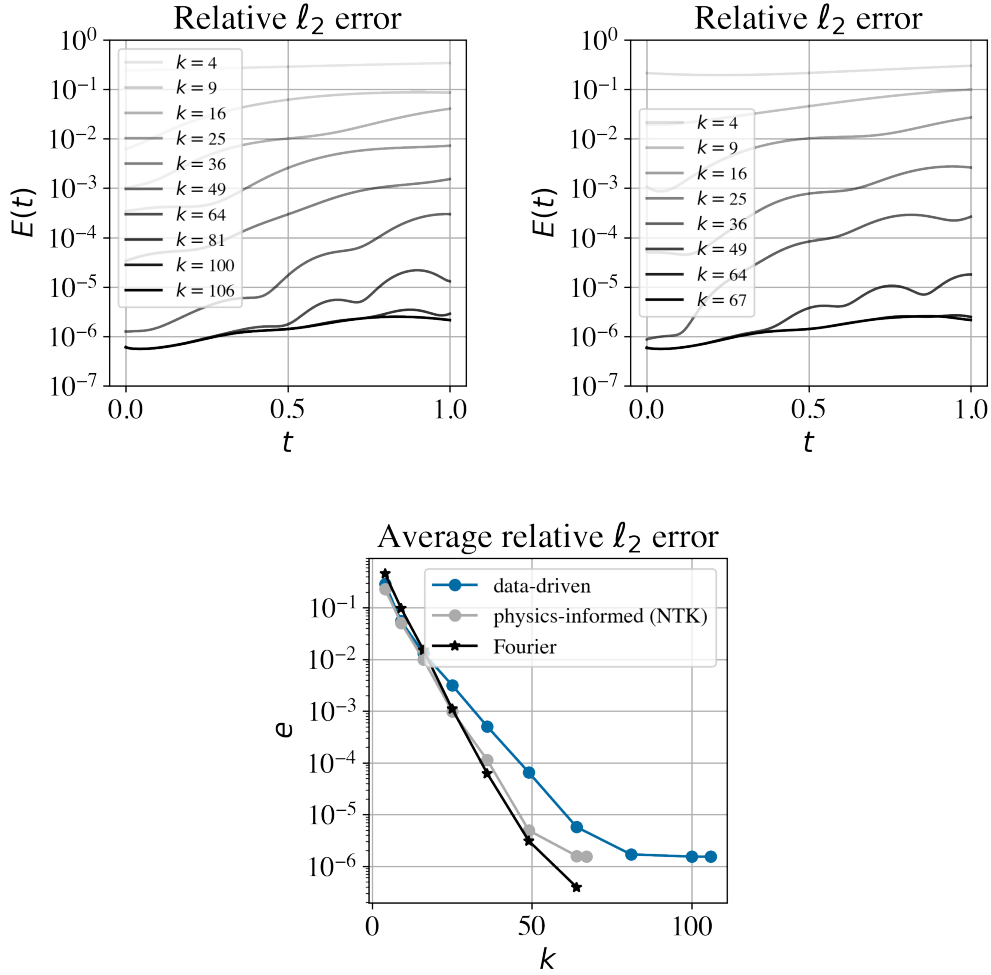


Figure 12: (Top left) Relative data-driven, (top right) relative physics-informed, and (bottom) average relative ℓ_2 test sample errors for random test sample initial condition with k custom basis functions for viscous Burgers with $\nu = 0.1$.

3.2.2 $\nu = 0.001$ and $\nu = 0.0001$

Now we turn to viscous Burgers with a lower viscosity, where physics-informed DeepONets struggle to train well, particularly without the NTK [29]. Consider the viscous Burgers benchmark investigated in [20, 30] with initial conditions generated from a GRF $\sim \mathcal{N}(0, 25^2(-\Delta + 5^2 I)^{-4})$ on $(x, t) \in (0, 1) \times (0, 1)$ with periodic boundary conditions. For calculating errors, the testing dataset generated using a Fourier spectral method from [29] is used. The models are trained using moderate local NTK adaptive weights with the modified DeepONet architecture [29]. First, consider viscosity $\nu = 0.001$. The physics-informed DeepONet prediction for this viscosity results in an

average relative ℓ_2 error of $4.48\% \pm 6.12\%$ across 100 independent test samples. Figure 13 shows an independent test sample and the physics-informed DeepONet prediction.

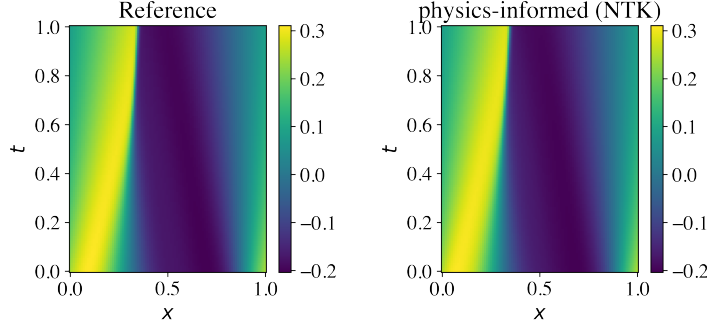


Figure 13: (Left) Numerical reference solution field and (right) physics-informed DeepONet prediction for viscous Burgers with $\nu = 0.001$.

We can exploit the well-trained physics-informed DeepONet for $\nu = 0.001$ in initializing a DeepONet model designed to approximate a more difficult problem. Specifically, we effectively fine-tune the trained parameters for viscous Burgers with an even lower viscosity. Consider viscosity $\nu = 0.0001$. Initializing the physics-informed DeepONet from the trained $\nu = 0.001$ parameters (transfer initialization) results in an improved prediction compared to random initialization. Shown in Table 5, the average relative ℓ_2 error from a physics-informed DeepONet initialized randomly for $\nu = 0.0001$ is over 13%. When initializing the physics-informed DeepONet for solving viscous Burgers with $\nu = 0.0001$ with the trained parameters from $\nu = 0.001$, this error decreases to almost 7%. Figure 14 shows the numerical reference solution field with the two physics-informed DeepONet predictions (random initialization and transfer initialization).

Initialization	Average relative ℓ_2 error
Random (NTK)	$13.67\% \pm 7.28\%$
Transfer (NTK) from $\nu = 0.001$	$7.03\% \pm 4.94\%$

Table 5: Average errors across 100 test samples for viscous Burgers with $\nu = 0.0001$.

Figure 15 shows the decay of the singular values and the expansion coefficients for the physics-informed DeepONets, with $\nu = 0.001$ as well as $\nu = 0.0001$ with random and transfer initialization. The expansion coefficients of all the trained models decay to machine precision, again showing that the models are training effectively. The decay of the singular values show the degrees of freedom that are important in capturing the solution space. For non-smooth problems, there is often more information (i.e., more basis functions) needed to learn this solution space. The physics-informed model for $\nu = 0.0001$ trained from the random initialization does not include all the modes required to represent this space, evidenced by the lower rank compared with the $\nu = 0.001$ problem. When the $\nu = 0.0001$ problem is initialized from the trained parameters from the $\nu = 0.001$ problem, we see the decay of the singular values being slower, meaning more basis functions are required to contain the information necessary to represent the solution.

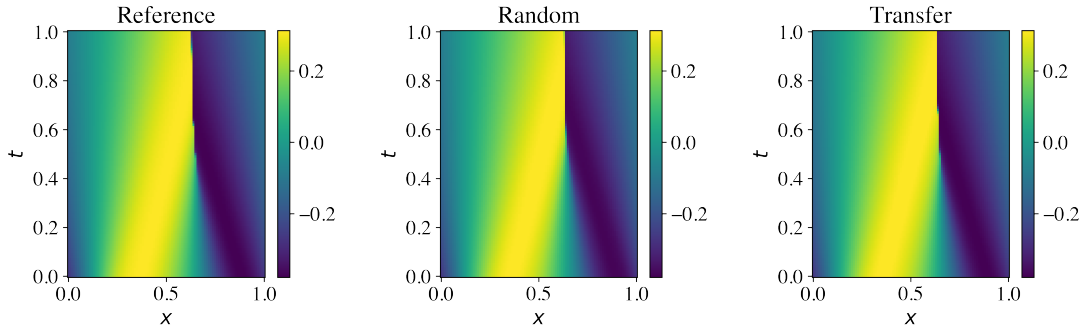


Figure 14: (Left) Numerical reference solution field, (middle) physics-informed using random initialization, and (right) physics-informed using transfer initialization DeepONet predictions for viscous Burgers with $\nu = 0.0001$.

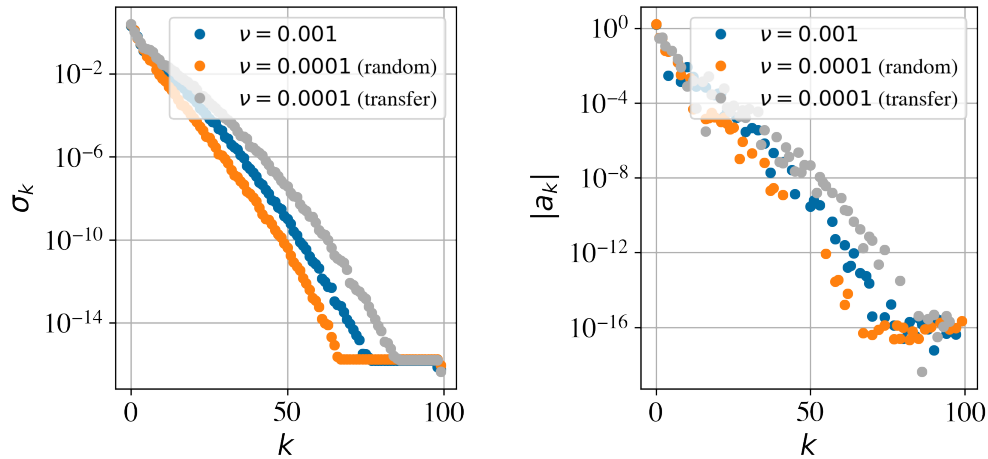


Figure 15: (Left) Singular values and (right) expansion coefficients for physics-informed DeepONets for different viscosities and initializations for $e^{\sin(x)}$ for viscous Burgers on $x \in (0, 1)$.

A sample of the custom basis functions is shown in Figure 16. Following [23], the custom basis functions are constructed at both $t = 0$ (solid) and $t = 1$ (dashed), i.e., “frozen-in-time” at the beginning (initial) and end (final) of the temporal domain. If the physics-informed DeepONet is effective in representing the solution space, we would expect the basis functions to change in time. For the $\nu = 0.001$ model, we see substantial shift between the initial and final basis functions across the spatial domain. For the $\nu = 0.0001$ model that is randomly initialized, the initial and final basis functions do not show significant shift in the spatial domain. However, for the $\nu = 0.0001$ with transfer initialization, there is noticeable shift away from the starting parameters from $\nu = 0.001$, toward functions that better represent the harder problem of $\nu = 0.0001$. This shows

the underlying fine-tuning process performed by the DeepONet in refining the parameters for the $\nu = 0.0001$ problem. The first 10 custom basis functions can be found in Appendix C.2.3.

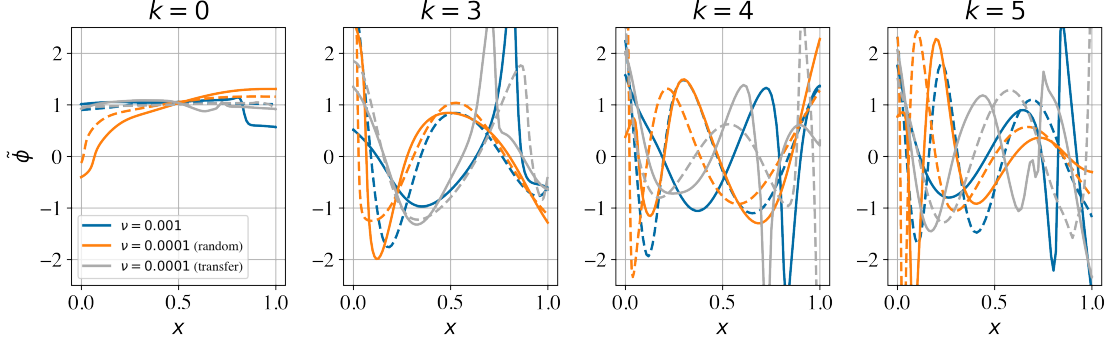


Figure 16: Custom basis functions, plotting with consistent boundaries $\bar{\phi}(x = 0 \text{ or } 1)$ (dashed: frozen-in-time at $t = 1$) for viscous Burgers on $x \in (0, 1)$.

3.3 Korteweg-de Vries

Lastly, we use transfer learning for initializing physics-informed DeepONets across different, but related, PDEs. Consider the Korteweg-de Vries equation

$$\frac{\partial s}{\partial t} + s \frac{\partial s}{\partial x} + \delta^2 \frac{\partial^3 s}{\partial x^3} = 0 \quad (19)$$

on $(x, t) \in (0, 2\pi) \times (0, 1)$ with periodic boundary conditions. The input to the branch network is the initial condition $s(x, 0) = u(x)$. The solution field is computed using a Fourier pseudo-spectral method. The strength of dispersion coefficient is $\delta = 0.1$. The data-driven and physics-informed DeepONets use the modified DeepONet architecture [29]. The physics-informed DeepONet can be initialized from the trained physics-informed parameters from viscous Burgers (transfer) on the same domain. Note that this domain is different than in Sec. 3.2.2. The domain in Section 3.2.2 was chosen to provide a comparison with existing papers [29, 30]. The relationship between viscous Burgers and Korteweg-de Vries is in the strengths of the viscous term and dispersive term. The physics-informed DeepONets use local CK adaptive weights. For this problem, CK weights demonstrated better performance compared to NTK weights. Figure 17 shows the reference solution field generated by the Fourier method for one independent test sample initial condition and the predictions from the physics-informed DeepONets initialized randomly and initialized with the trained parameters from the viscous Burgers $\nu = 0.0001$ problem. The viscous Burgers parameters for $\nu = 0.0001$ are themselves transfer initialized from the $\nu = 0.001$ problem with local CK adaptive weights. Shown in Table 6, the average relative ℓ_2 error when randomly initialized is 3.92%. When initializing the physics-informed DeepONet for solving Korteweg-de Vries with the trained parameters from viscous Burgers, this error decreases to 3.29% across 100 test samples. The larger standard deviations point to increased variability in the predictions from the physics-informed model.

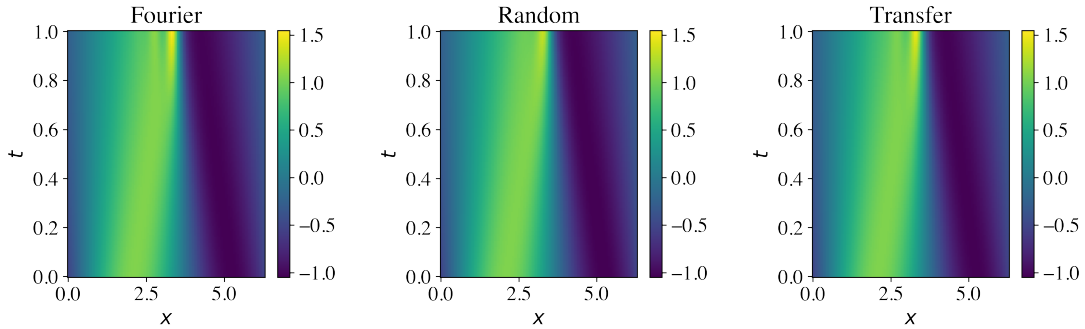


Figure 17: (Left) Fourier reference solution field, (middle) physics-informed using random initialization, and (right) physics-informed using transfer initialization DeepONet predictions for Korteweg-de Vries.

Initialization	Average relative ℓ_2 error
Random (CK)	$3.92\% \pm 6.80\%$
Transfer (CK) from viscous Burgers with $\nu = 0.0001$	$3.29\% \pm 5.94\%$

Table 6: Average errors across 100 test samples for Korteweg-de Vries from transfer initialized viscous Burgers with $\nu = 0.0001$.

Figure 18 shows the decay of the singular values and the expansion coefficients for the data-driven and physics-informed DeepONets, with random and transfer initialization. The expansion coefficients of the data-driven model and physics-informed model using the transfer initialization decay to machine precision, again showing that the models are training effectively. However, the expansion coefficients of the physics-informed model initialized randomly do not drop all the way to machine precision, meaning that it is not training effectively. The decay of the singular values show the degrees of freedom that are important in capturing the solution space. The singular values of the randomly initialized physics-informed model decays much faster, showing that it is not including all the modes necessary to represent the solution space. When initialized from the trained parameters from the viscous Burgers problem, we see the decay of the singular values being significantly slower, meaning more basis functions are required to capture the information necessary to represent the solution, and that the model is learning effectively.

A sample of the custom basis functions is shown in Figure 19. We expect the basis functions to change in time. For the data-driven custom basis functions, we see substantial shift between the initial and final basis functions across the spatial domain. For physics-informed model that is randomly initialized, the initial and final basis functions show almost no change in time. However, for the physics-informed model with transfer initialization, there is a substantial shift toward functions that better represent the Korteweg-de Vries problem, evidenced by the better agreement with the data-driven custom basis functions. This demonstrates the underlying fine-tuning process performed by the DeepONet across different PDEs. The first 10 custom basis functions can be found in Appendix C.3.

For Korteweg-de Vries, randomly initializing the DeepONet parameters is shown to result in

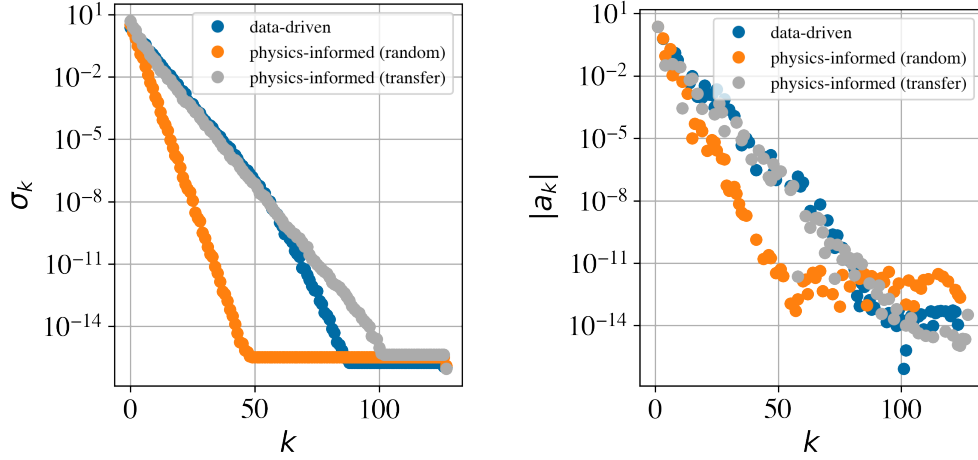


Figure 18: (Left) Singular values and (right) expansion coefficients for data-driven and physics-informed DeepONets for different initializations for $e^{\sin(x)}$ for Korteweg-de Vries.

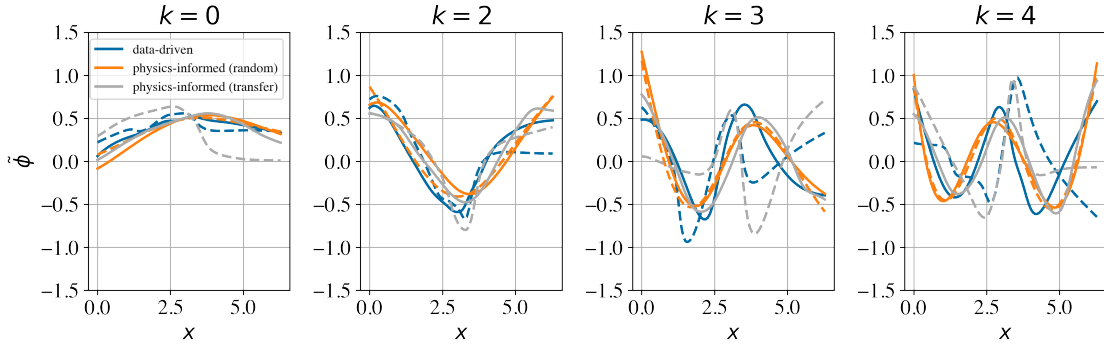


Figure 19: Custom basis functions, plotting with consistent boundaries $\tilde{\phi}(x = 0 \text{ or } 2\pi)$ (dashed: frozen-in-time at $t = 1$) for Korteweg-de Vries.

less effective basis functions in time and space. The decay of the singular values as well as the decay of the expansion coefficients needs to be considered when assessing how well a physics-informed DeepONet is learning. Finally, there are benefits to using transfer learning to initialize a DeepONet for a more difficult PDE from a related PDE, such as learning more effective basis functions that can be used in a spectral method.

4 Conclusions

In this work, we evaluated quantities of interest (e.g., singular values, expansion coefficients) toward assessing the performance of a physics-informed DeepONet. Further, we extracted basis functions from the trained models to develop further understanding toward the universality of the learning process of DeepONets. The basis functions extracted from the improved physics-informed DeepONets are shown to provide potential model reduction benefits when used to evolve the approximation using a spectral approach for advection-diffusion and viscous Burgers with $\nu = 0.1$. Lastly, we proposed a transfer learning approach for improving training for physics-informed DeepONets between parameters of the same PDE as well as across different, but related, PDEs. This approach was demonstrated on problems where physics-informed DeepONets struggle to train, including viscous Burgers with $\nu = 0.0001$, and resulted in significant reduction in error and more expressive learned basis functions. These results contribute to the promising methodology of discovering the solutions of more difficult problems starting from the solutions of easier, but related, problems [13]. Future work includes further investigation toward the performance of physics-informed DeepONets and the learned basis functions using different adaptive weighting schemes.

Acknowledgements

This project was completed with support from the U.S. Department of Energy, Advanced Scientific Computing Research program, under the Scalable, Efficient and Accelerated Causal Reasoning Operators, Graphs and Spikes for Earth and Embedded Systems (SEA-CROGS) project (Project No. 80278). The computational work was performed using PNNL Institutional Computing at Pacific Northwest National Laboratory. Pacific Northwest National Laboratory (PNNL) is a multi-program national laboratory operated for the U.S. Department of Energy (DOE) by Battelle Memorial Institute under Contract No. DE-AC05-76RL01830.

This material is based upon work supported by the U.S. Department of Energy, Office of Science, Office of Advanced Scientific Computing Research, Department of Energy Computational Science Graduate Fellowship under Award Number DE-SC0023112. This report was prepared as an account of work sponsored by an agency of the United States Government. Neither the United States Government nor any agency thereof, nor any of their employees, makes any warranty, express or implied, or assumes any legal liability or responsibility for the accuracy, completeness, or usefulness of any information, apparatus, product, or process disclosed, or represents that its use would not infringe privately owned rights. Reference herein to any specific commercial product, process, or service by trade name, trademark, manufacturer, or otherwise does not necessarily constitute or imply its endorsement, recommendation, or favoring by the United States Government or any agency thereof. The views and opinions of authors expressed herein do not necessarily state or reflect those of the United States Government or any agency thereof.

A Training data and network parameters

Physics-informed DeepONets are trained with the hyperbolic tangent activation function. The Adam optimizer with learning rate 0.001 is used with an exponential decay scheduler. Table 7 shows the input function spaces and domains for the selected test cases. For advection-diffusion, some function $f(x)$ is sampled from a mean zero Gaussian random field (GRF) with covariance kernel

$$\kappa_l(f(x_1), f(x_2)) = \exp\left(\frac{-\|f(x_1) - f(x_2)\|^2}{2l^2}\right) \quad (20)$$

for some length scale l to generate the random training and testing inputs, as in [23]. Some sample inputs are plotted in Figure 20. Table 8 specifies the training hyperparameters for each test case, and Table 9 shows the network sizes.

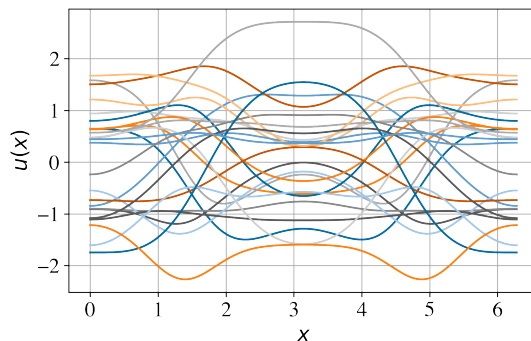


Figure 20: 25 example functions sampled from the GRF, $f(\sin^2(x/2))$ and $l = 0.5$.

	Function/Kernel	Domain
Advection-diffusion	$f(\sin^2(x/2)), l = 0.5$	$x \in (0, 2\pi)$
Viscous Burgers	$\mathcal{N}(0, 25^2(-\Delta + 5^2I)^{-4})$	$x \in (0, 1)$
Korteweg-de Vries	$c(-a \sin(x) + b \cos(x))$	$a, b \in \mathcal{U}[0, 1)$ $c \in \mathcal{U}[-1, 1)$ $x \in (0, 2\pi)$

Table 7: Input function space $u(x)$ [23, 28].

	m	Train	Test	P	Batch size	Epochs
Advection-diffusion	128	500	100	128	1000	200000
Viscous Burgers	101	500	100	101	14000	200000
Korteweg-de Vries	128	500	100	128	16384	200000

Table 8: Hyper-parameter settings.

	Trunk width	Trunk depth	Branch width	Branch depth
Advection-diffusion	128	4	128	3
Viscous Burgers	100	7	100	7
Korteweg-de Vries	128	6	128	5

Table 9: Network sizes.

B Viscous Burgers $x \in (0, 2\pi)$

Consider viscous Burgers on the domain $x \in (0, 2\pi)$. The initial conditions are generated from the GRF in Appendix A used for advection-diffusion. First, consider viscosity $\nu = 0.001$. The physics-informed DeepONet is trained with local NTK adaptive weights and results in an average relative ℓ_2 error of $3.84\% \pm 3.34\%$ across 100 independent test samples computed using a Fourier pseudo-spectral method. Figure 21 shows an independent test sample and the physics-informed DeepONet prediction. The widths of the trunk and branch nets are 128. The depths of the trunk and branch nets are 6 and 5, respectively, to enable transfer initialization to the Korteweg-de Vries problem.

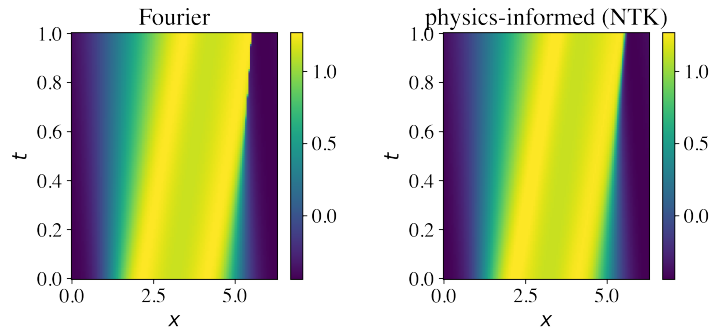


Figure 21: (Left) Fourier reference solution field and (right) physics-informed DeepONet prediction for $\nu = 0.001$.

Now, consider viscosity $\nu = 0.0001$. Initializing the physics-informed DeepONet with local NTK adaptive weights from the trained $\nu = 0.001$ parameters (transfer initialization) results in an improved prediction compared to random initialization. Shown in Table 10, the average relative ℓ_2 error from a physics-informed DeepONet initialized randomly for $\nu = 0.0001$ is 3.15%.

When initializing the physics-informed DeepONet for solving viscous Burgers with $\nu = 0.0001$ with the trained parameters from $\nu = 0.001$, this error decreases to 2.24%. Figure 22 shows the decay of the singular values and the expansion coefficients for the physics-informed DeepONets. The expansion coefficients decay to machine precision, meaning that they are training effectively. However, the transfer model utilizes more modes to represent the solution space, compared to the randomly initialized model that has a lower rank than the less difficult problem of $\nu = 0.001$, meaning that it is not including all the necessary modes. A sample of the custom basis functions is shown in Figure 23, “frozen-in-time” at both $t = 0$ and $t = 1$. Qualitatively, the solution fields for viscous Burgers with $\nu = 0.001$ and $\nu = 0.0001$ look similar, which is reflected in the basis functions, particularly in capturing the location of the shock. The parameters are given a “warm start” in moving toward basis functions that are more representative of the solution space, rather than starting from scratch with a random initialization. The first 10 custom basis functions can be found in Appendix C.2.2.

Initialization	Average relative ℓ_2 error
Random (NTK)	$3.15\% \pm 2.35\%$
Transfer (NTK) from $\nu = 0.001$	$2.24\% \pm 1.63\%$

Table 10: Average errors across 5 test samples for viscous Burgers with $\nu = 0.0001$.

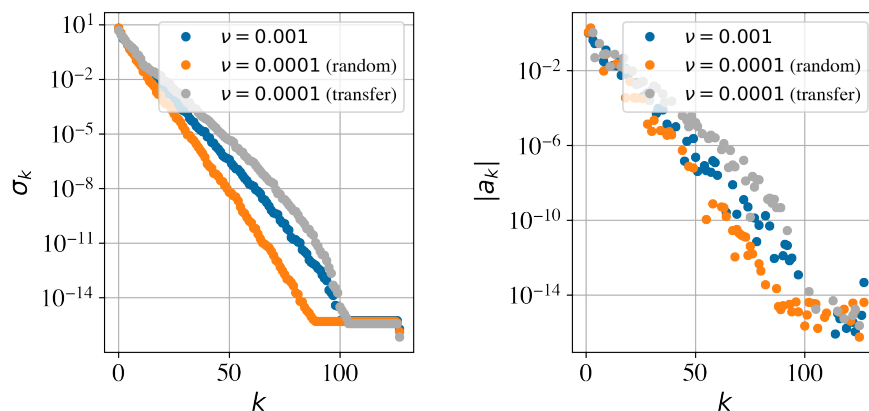


Figure 22: (Left) Singular values and (right) expansion coefficients for physics-informed DeepONets for different viscosities and initializations for $e^{\sin(x)}$ for viscous Burgers on $x \in (0, 2\pi)$.

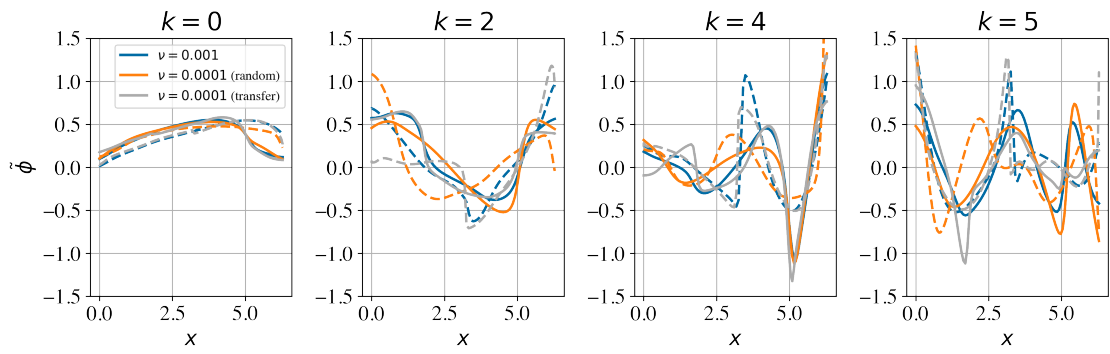


Figure 23: Custom basis functions, plotting with consistent boundaries $\tilde{\phi}(x = 0 \text{ or } 2\pi)$ (dashed: frozen-in-time at $t = 1$) for viscous Burgers on $x \in (0, 2\pi)$.

C Basis functions

C.1 Advection-diffusion

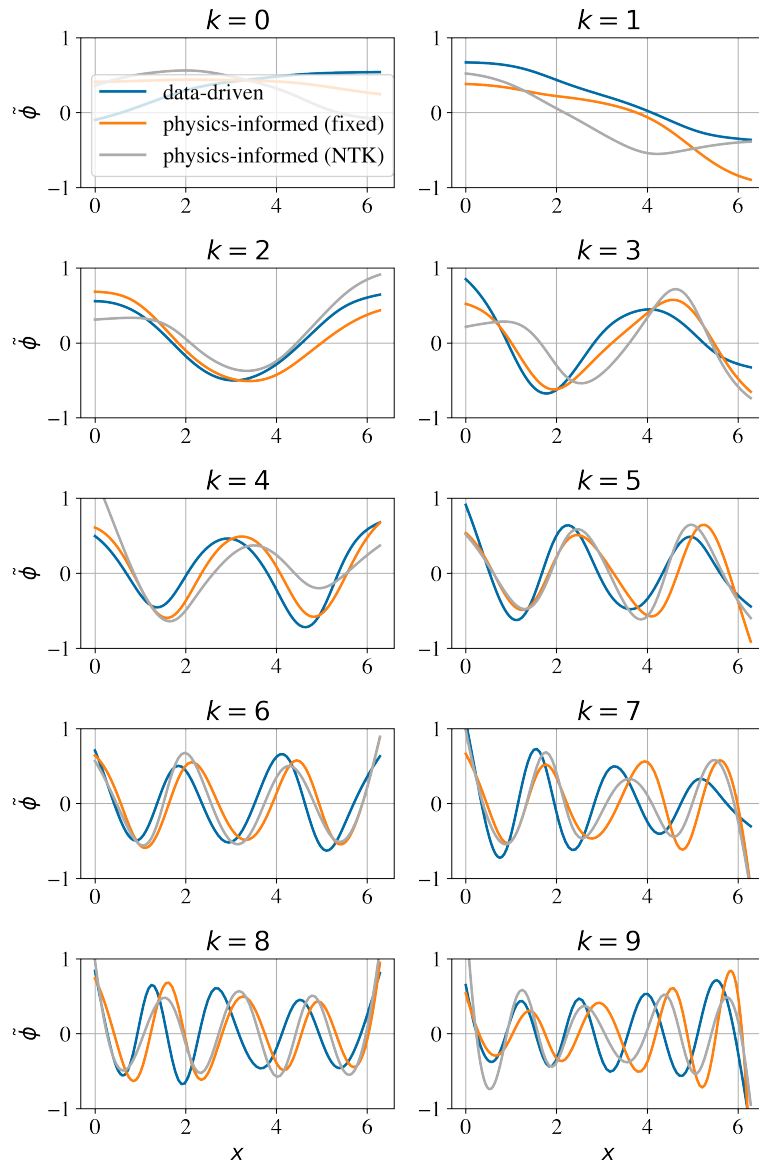


Figure 24: First 10 custom basis functions, plotting with consistent boundaries $\tilde{\phi}(x = 0 \text{ or } 2\pi)$ for advection-diffusion.

C.2 Viscous Burgers

C.2.1 $\nu = 0.1$ on $x \in (0, 2\pi)$

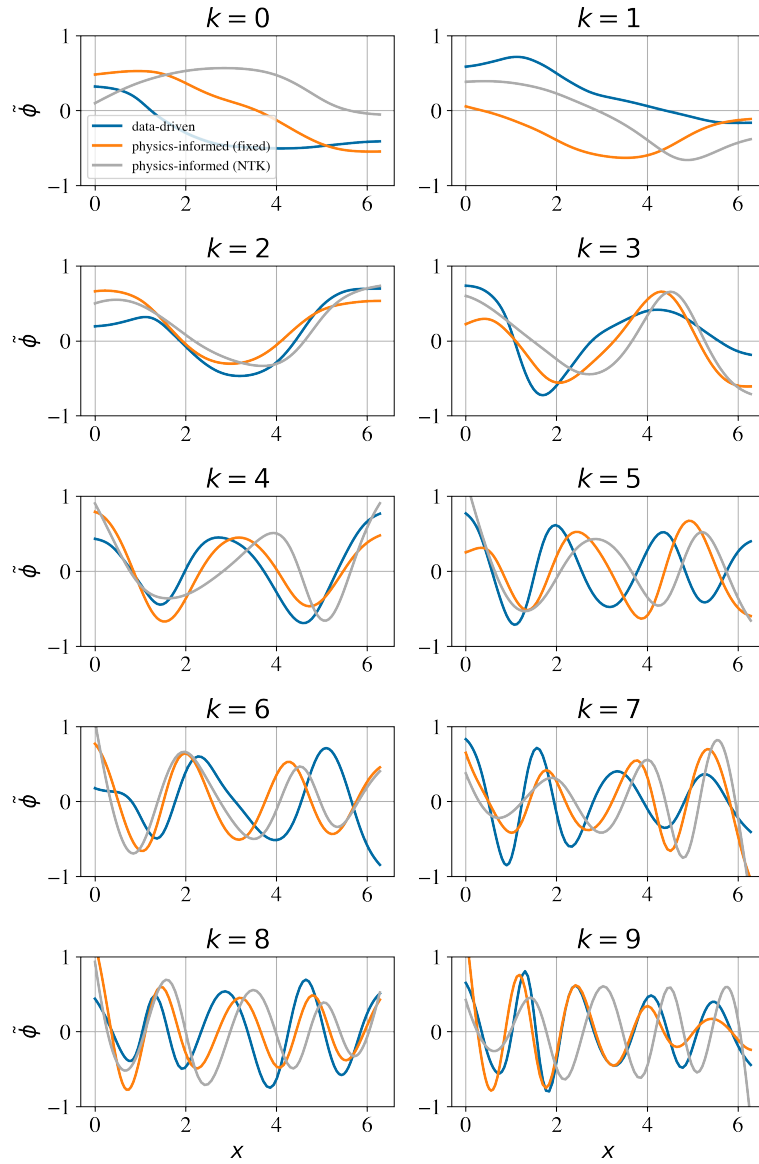


Figure 25: First 10 custom basis functions, plotting with consistent boundaries $\tilde{\phi}(x = 0 \text{ or } 2\pi)$ for viscous Burgers with $\nu = 0.1$.

C.2.2 $\nu = 0.001$ and $\nu = 0.0001$ on $x \in (0, 2\pi)$

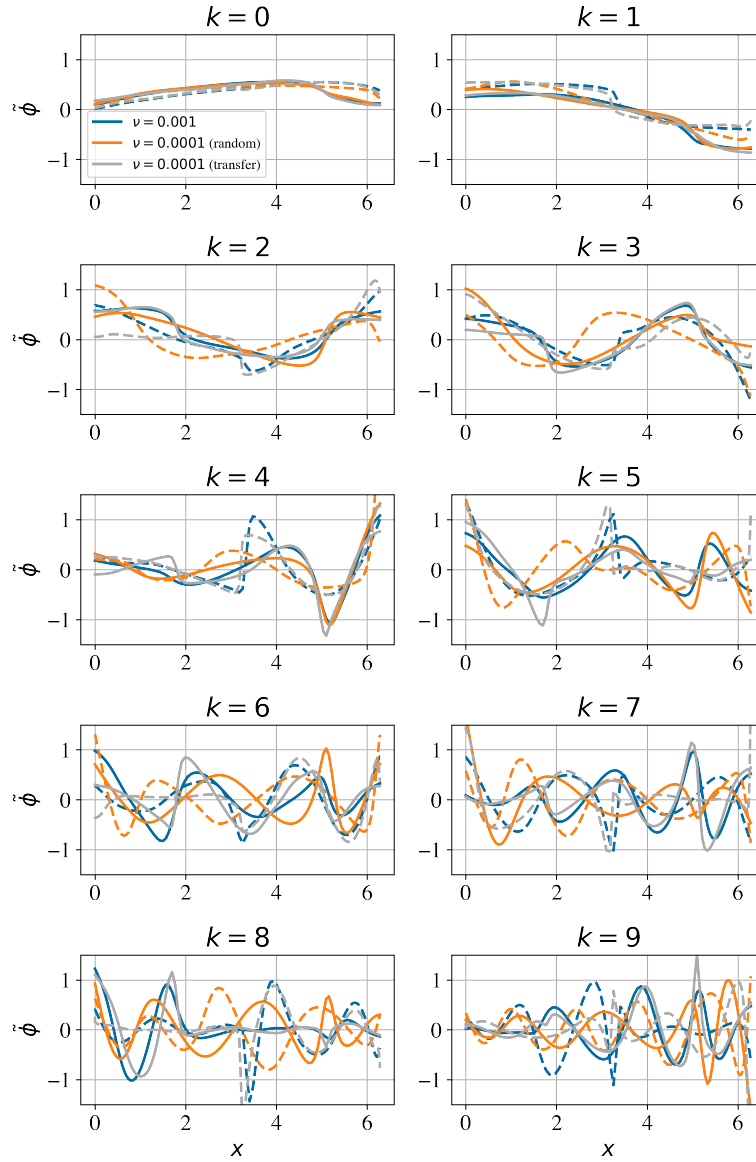


Figure 26: First 10 custom basis functions, plotting with consistent boundaries $\tilde{\phi}(x = 0 \text{ or } 2\pi)$ (dashed: “frozen-in-time” at $t = 1$) for viscous Burgers with $\nu = 0.001$ and $\nu = 0.0001$.

C.2.3 $\nu = 0.001$ and $\nu = 0.0001$ on $x \in (0, 1)$

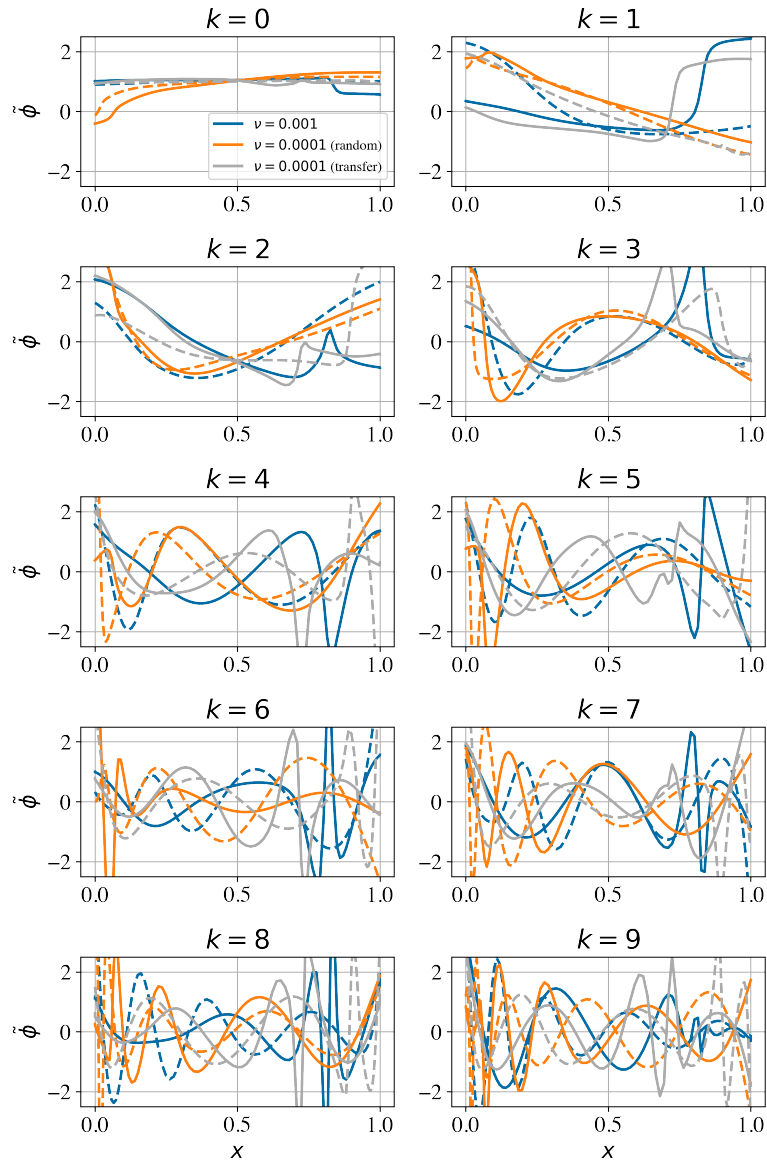


Figure 27: First 10 custom basis functions, plotting with consistent boundaries $\tilde{\phi}(x = 0 \text{ or } 1)$ (dashed: “frozen-in-time” at $t = 1$) for viscous Burgers with $\nu = 0.001$ and $\nu = 0.0001$.

C.3 Korteweg-de Vries

C.3.1 Random initialization

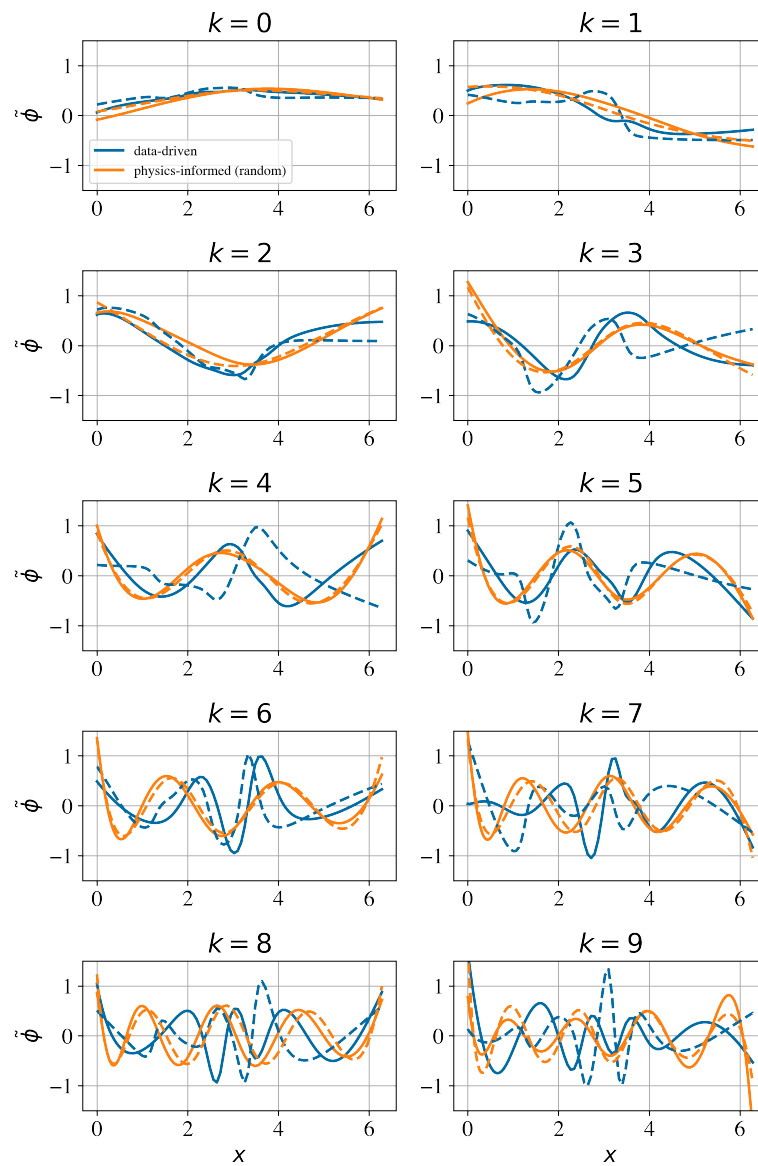


Figure 28: First 10 custom basis functions from random initialization, plotting with consistent boundaries $\tilde{\phi}(x = 0 \text{ or } 2\pi)$ (dashed: “frozen-in-time” at $t = 1$) for Korteweg-de Vries.

C.3.2 Transfer initialization

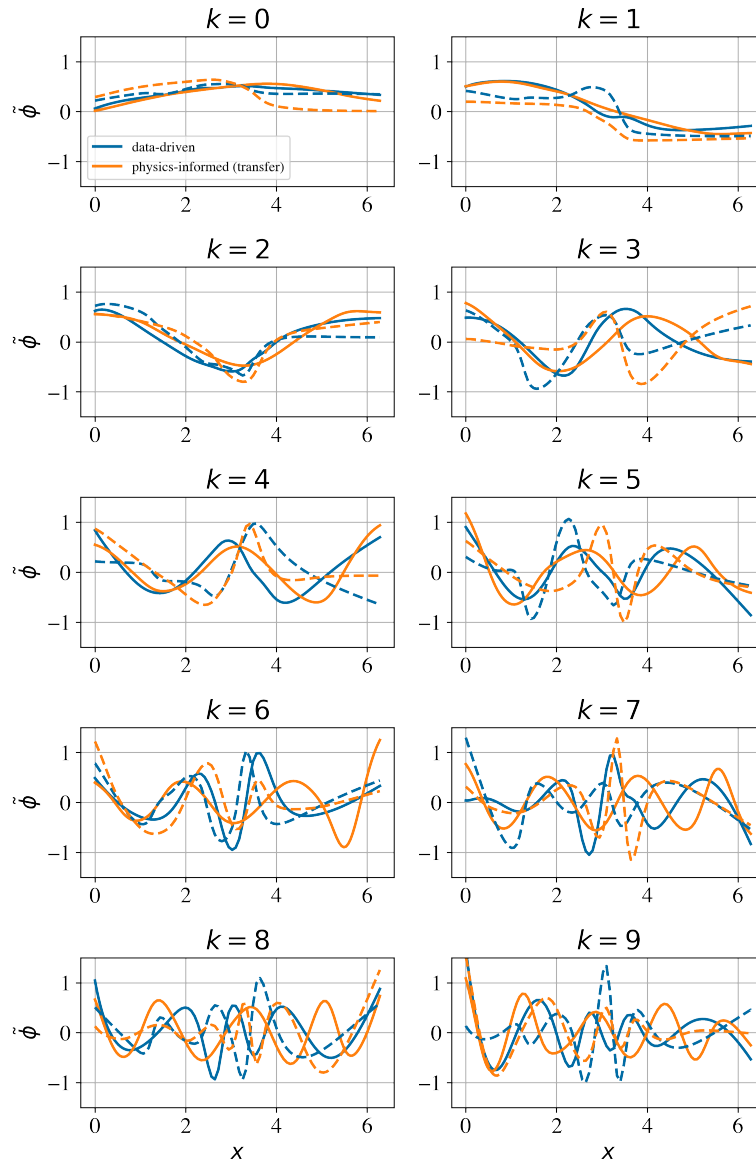


Figure 29: First 10 custom basis functions from transfer initialization with viscous Burgers, plotting with consistent boundaries $\tilde{\phi}(x = 0 \text{ or } 2\pi)$ (dashed: “frozen-in-time” at $t = 1$) for Korteweg-de Vries.

D Training cost

Computational costs for training physics-informed DeepONets with moderate local adaptive weights for the viscous Burgers benchmark case with $\nu = 0.001$ from Section 3.2.2 are included in Table 11. All models were trained on 1 NVIDIA P100 GPU on the PNNL Institutional Computing Cluster (Marianas). Training times are averaged over 5 independent runs.

	Training time	Average relative ℓ_2 error
Neural tangent kernel (NTK)	7 hr 56 min	4.48% \pm 6.12%
Conjugate kernel (CK)	3 hr 11 min	7.56% \pm 7.63%

Table 11: Training costs for physics-informed DeepONet for viscous Burgers with $\nu = 0.001$.

E Error definitions

In the error computations, \hat{s} is the approximation and s is the “ground truth” solution.

E.1 Relative ℓ_2 error

$$E(t_n) = \frac{\|\hat{s}(x, t_n) - s(x, t_n)\|_2}{\|s(x, t_n)\|_2} \quad (21)$$

E.2 Average error

$$e = \frac{1}{T} \int_0^T E(t) dt \quad (22)$$

where the integral is approximated using the trapezoidal rule [23].

References

- [1] Mark Alber et al. “Integrating Machine Learning and Multiscale Modeling—Perspectives, Challenges, and Opportunities in the Biological, Biomedical, and Behavioral Sciences”. In: *npj Digital Medicine* 2.1 (Nov. 2019), pp. 1–11. ISSN: 2398-6352. DOI: 10.1038/s41746-019-0193-y. (Visited on 11/06/2024).
- [2] Zeyuan Allen-Zhu, Yuanzhi Li, and Zhao Song. “A Convergence Theory for Deep Learning via Over-Parameterization”. In: *Proceedings of the 36th International Conference on Machine Learning*. PMLR, May 2019, pp. 242–252. (Visited on 11/09/2024).
- [3] S. Bozinovski and A. Fulgosi. “The influence of pattern similarity and transfer learning upon training of a base perceptron b2”. In: *Proceedings of Symposium Informatica 3* (1976), pp. 121–126.
- [4] Tianping Chen and Hong Chen. “Universal Approximation to Nonlinear Operators by Neural Networks with Arbitrary Activation Functions and Its Application to Dynamical Systems”. In: *IEEE Transactions on Neural Networks* 6.4 (July 1995), pp. 911–917. ISSN: 1941-0093. DOI: 10.1109/72.392253. (Visited on 09/02/2024).
- [5] Alexis Conneau et al. *Supervised Learning of Universal Sentence Representations from Natural Language Inference Data*. July 2018. DOI: 10.48550/arXiv.1705.02364. arXiv: 1705.02364. (Visited on 11/09/2024).
- [6] Chuong B Do and Andrew Y Ng. “Transfer Learning for Text Classification”. In: *Advances in neural information processing systems* (2005).
- [7] Simon Du et al. “Gradient Descent Finds Global Minima of Deep Neural Networks”. In: *Proceedings of the 36th International Conference on Machine Learning*. PMLR, May 2019, pp. 1675–1685. (Visited on 11/09/2024).
- [8] Zhou Fan and Zhichao Wang. “Spectra of the Conjugate Kernel and Neural Tangent Kernel for Linear-Width Neural Networks”. In: *Advances in Neural Information Processing Systems*. Vol. 33. Curran Associates, Inc., 2020, pp. 7710–7721. (Visited on 11/12/2024).
- [9] Xavier Glorot and Yoshua Bengio. “Understanding the Difficulty of Training Deep Feedforward Neural Networks”. In: *Proceedings of the Thirteenth International Conference on Artificial Intelligence and Statistics*. JMLR Workshop and Conference Proceedings, Mar. 2010, pp. 249–256. (Visited on 11/09/2024).
- [10] Ian Goodfellow, Yoshua Bengio, and Aaron Courville. *Deep Learning*. MIT Press, 2016.
- [11] Somdatta Goswami et al. “Deep Transfer Operator Learning for Partial Differential Equations under Conditional Shift”. In: *Nature Machine Intelligence* 4.12 (Dec. 2022), pp. 1155–1164. ISSN: 2522-5839. DOI: 10.1038/s42256-022-00569-2. (Visited on 11/09/2024).
- [12] Amanda A Howard et al. “The conjugate kernel for efficient training of physics-informed deep operator networks”. In: *ICLR 2024 Workshop on AI4DifferentialEquations In Science*. 2024.
- [13] Amanda A. Howard et al. “Stacked Networks Improve Physics-Informed Training: Applications to Neural Networks and Deep Operator Networks”. In: *Foundations of Data Science* (2024). DOI: 10.3934/fods.2024029.
- [14] Lin Hu et al. *Operator Transfer Learning for Physics Field Prediction on Complex Geometries with Limited Labelled Data*. SSRN Scholarly Paper. Rochester, NY, Oct. 2024. DOI: 10.2139/ssrn.4981813. (Visited on 11/16/2024).

- [15] Mohammadreza Iman, Hamid Reza Arabnia, and Khaled Rasheed. “A Review of Deep Transfer Learning and Recent Advancements”. In: *Technologies* 11.2 (Apr. 2023), p. 40. ISSN: 2227-7080. DOI: 10.3390/technologies11020040. (Visited on 11/09/2024).
- [16] Arthur Jacot, Franck Gabriel, and Clement Hongler. “Neural Tangent Kernel: Convergence and Generalization in Neural Networks”. In: *Advances in Neural Information Processing Systems*. Vol. 31. Curran Associates, Inc., 2018. (Visited on 11/09/2024).
- [17] Adar Kahana et al. “On the Geometry Transferability of the Hybrid Iterative Numerical Solver for Differential Equations”. In: *Computational Mechanics* 72.3 (Sept. 2023), pp. 471–484. ISSN: 1432-0924. DOI: 10.1007/s00466-023-02271-5. (Visited on 11/16/2024).
- [18] George Em Karniadakis et al. “Physics-Informed Machine Learning”. In: *Nature Reviews Physics* 3.6 (June 2021), pp. 422–440. ISSN: 2522-5820. DOI: 10.1038/s42254-021-00314-5. (Visited on 09/02/2024).
- [19] Varun Kumar et al. *Synergistic Learning with Multi-Task DeepONet for Efficient PDE Problem Solving*. Aug. 2024. arXiv: 2408.02198. (Visited on 11/16/2024).
- [20] Zongyi Li et al. *Fourier Neural Operator for Parametric Partial Differential Equations*. May 2021. DOI: 10.48550/arXiv.2010.08895. arXiv: 2010.08895. (Visited on 11/06/2024).
- [21] Tong Liu et al. “Exploring Transfer Learning to Reduce Training Overhead of HPC Data in Machine Learning”. In: *2019 IEEE International Conference on Networking, Architecture and Storage (NAS)*. Aug. 2019, pp. 1–7. DOI: 10.1109/NAS.2019.8834723. (Visited on 11/09/2024).
- [22] Lu Lu et al. “Learning Nonlinear Operators via DeepONet Based on the Universal Approximation Theorem of Operators”. In: *Nature Machine Intelligence* 3.3 (Mar. 2021), pp. 218–229. ISSN: 2522-5839. DOI: 10.1038/s42256-021-00302-5. (Visited on 05/29/2024).
- [23] Brek Meuris, Saad Qadeer, and Panos Stinis. “Machine-Learning-Based Spectral Methods for Partial Differential Equations”. In: *Scientific Reports* 13.1 (Jan. 2023), p. 1739. ISSN: 2045-2322. DOI: 10.1038/s41598-022-26602-3. (Visited on 05/08/2024).
- [24] Saad Qadeer et al. *Efficient Kernel Surrogates for Neural Network-Based Regression*. Jan. 2024. DOI: 10.48550/arXiv.2310.18612. arXiv: 2310.18612. (Visited on 11/06/2024).
- [25] Hoo-Chang Shin et al. “Deep Convolutional Neural Networks for Computer-Aided Detection: CNN Architectures, Dataset Characteristics and Transfer Learning”. In: *IEEE transactions on medical imaging* 35.5 (May 2016), pp. 1285–1298. ISSN: 1558-254X. DOI: 10.1109/TMI.2016.2528162.
- [26] Selvakumar Venkatasubbu and Sai Mani Krishna Sistla. “Harnessing the Power of Transfer Learning in Deep Learning Models”. In: *Journal of Knowledge Learning and Science Technology* ISSN: 2959-6386 (online) 1.1 (Jan. 2023), pp. 139–147. ISSN: 2959-6386. DOI: 10.60087/jklst.vol1.n1.p147. (Visited on 11/16/2024).
- [27] Sifan Wang and Paris Perdikaris. *Long-Time Integration of Parametric Evolution Equations with Physics-Informed DeepONets*. June 2021. DOI: 10.48550/arXiv.2106.05384. arXiv: 2106.05384. (Visited on 11/16/2024).
- [28] Sifan Wang, Shyam Sankaran, and Paris Perdikaris. “Respecting Causality for Training Physics-Informed Neural Networks”. In: *Computer Methods in Applied Mechanics and Engineering* 421 (Mar. 2024), p. 116813. ISSN: 0045-7825. DOI: 10.1016/j.cma.2024.116813. (Visited on 11/06/2024).

- [29] Sifan Wang, Hanwen Wang, and Paris Perdikaris. “Improved Architectures and Training Algorithms for Deep Operator Networks”. In: *J. Sci. Comput.* 92.2 (Aug. 2022). ISSN: 0885-7474. DOI: 10.1007/s10915-022-01881-0. (Visited on 11/06/2024).
- [30] Sifan Wang, Hanwen Wang, and Paris Perdikaris. “Learning the Solution Operator of Parametric Partial Differential Equations with Physics-Informed DeepONets”. In: *Science Advances* 7.40 (Sept. 2021), eabi8605. DOI: 10.1126/sciadv.abi8605. (Visited on 06/01/2024).
- [31] Sidi Wu. *Fine-Tuning DeepONets to Enhance Physics-informed Neural Networks for Solving Partial Differential Equations*. Oct. 2024. DOI: 10.48550/arXiv.2410.14134. arXiv: 2410.14134. (Visited on 11/09/2024).
- [32] Chen Xu et al. “A multi-fidelity deep operator network (DeepONet) for fusing simulation and monitoring data: Application to real-time settlement prediction during tunnel construction”. In: *Engineering Applications of Artificial Intelligence* 133 (2024), p. 108156.
- [33] Wuzhe Xu, Yulong Lu, and Li Wang. “Transfer Learning Enhanced DeepONet for Long-Time Prediction of Evolution Equations”. In: *Proceedings of the AAAI Conference on Artificial Intelligence* 37.9 (June 2023), pp. 10629–10636. ISSN: 2374-3468. DOI: 10.1609/aaai.v37i9.26262. (Visited on 11/16/2024).
- [34] Jason Yosinski et al. “How Transferable Are Features in Deep Neural Networks?” In: *Advances in Neural Information Processing Systems*. Vol. 27. Curran Associates, Inc., 2014. (Visited on 11/09/2024).
- [35] Zecheng Zhang et al. *DeepONet as a Multi-Operator Extrapolation Model: Distributed Pretraining with Physics-Informed Fine-Tuning*. 2024. arXiv: 2411.07239 [cs.LG]. URL: <https://arxiv.org/abs/2411.07239>.